Selective nucleotide-release from dense-core granules in insulin-secreting cells

Stefanie Obermüller[1], Anders Lindqvist[1], Jovita Karanauskaite[1,2], Juris Galvanovskis[2], Patrik Rorsman[1,2] and Sebastian Barg[1,3,*]

[1]Department of Experimental Medicinal Sciences, Lund University, BMC B11, SE-221 84 Lund, Sweden
[2]OCDEM, Nuffield Department of Clinical Medicine, University of Oxford, Churchill Hospital, Oxford, OX3 7LJ, UK
[3]Vollum Institute, Oregon Health and Sciences University, 3181 SW Sam Jackson Park Road, Portland OR, 97210, USA
*Author for correspondence (e-mail: bargs@ohsu.edu)

Accepted 17 June 2005
Journal of Cell Science 118, 4271-4282 Published by The Company of Biologists 2005
doi:10.1242/jcs.02549

Summary

Secretory granules of insulin-secreting cells are used to store and release peptide hormones as well as low-molecular-weight compounds such as nucleotides. Here we have compared the rate of exocytosis with the time courses of nucleotide and peptide release by a combination of capacitance measurements, electrophysiological detection of ATP release and single-granule imaging. We demonstrate that the release of nucleotides and peptides is delayed by ~0.1 and ~2 seconds with respect to membrane fusion, respectively. We further show that in up to 70% of the cases exocytosis does not result in significant release of the peptide cargo, likely because of a mechanism that leads to premature closure of the fusion pore. Release of nucleotides and protons occurred regardless of whether peptides were secreted or not. These observations suggest that insulin-secreting cells are able to use the same secretory vesicles to release small molecules either alone or together with the peptide hormone.

Key words: Exocytosis, Endocytosis, Fusion pore, Insulin, Hormone, Kiss-and-run, Secretion

Introduction

Pancreatic B-cells and other (neuro-)endocrine cells use large dense-core vesicles (LDCVs or granules) to store and release a variety of peptide hormones, such as insulin. In addition, these granules contain high concentrations of low-molecular-weight transmitter molecules, such as amino acids, nucleotides and amines (Hutton, 1994). Release of any granule cargo requires regulated exocytosis, which has classically been envisioned as 'full fusion' of the granule with the plasma membrane (Heuser and Reese, 1973; Viveros et al., 1969). In this mode of exocytosis, the granule fuses with the plasmalemma and the two membranes mix completely. Consequently, the entire granule content is discharged into the extracellular space, which is consistent with the finding that the mixture of secreted products is similar to that of the granule cargo (Detimary et al., 1995; Kirshner et al., 1966).

In an alternative mode of exocytosis, originally proposed for synaptic vesicles (Ceccarelli et al., 1973), a transient pore forms between the vesicle lumen and the extracellular space. This pore permits release of transmitter and uptake of tracer molecules, but reseals rapidly to reestablish the integrity of the original secretory vesicle (transient fusion or 'kiss-and-run'). A hallmark of neuronal 'kiss-and-run' exocytosis is the absence of lipid mixing between vesicle and plasma membrane (Aravanis et al., 2003). A similar mechanism may exist in dense-core granule exocytosis. Indeed, live-cell imaging of fluorescently labeled granule proteins led to the conclusion that a fraction of granules can retain their identity during exocytosis, and that these granules reseal later (Holroyd et al., 2002; Perrais et al., 2004; Taraska et al., 2003; Tsuboi et al., 2004). However, in these granules a lipid marker as well as some integral membrane proteins dispersed from the granular membrane into the plasma membrane (Taraska and Almers, 2004; Tsuboi and Rutter, 2003), indicating partial mixing of the two membranes. To indicate this difference of transient granule exocytosis to neuronal 'kiss-and-run' exocytosis, the term 'cavicapture' has been introduced (Taraska et al., 2003).

Fusion of a secretory granule with the plasma membrane begins with the formation of a narrow fusion pore (Breckenridge and Almers, 1987; Zimmerberg et al., 1987). The fusion pore has an initial diameter of 2-3 nm that widens and fluctuates in diameter, but may close again as long as it stays below a critical threshold of 10-20 nm (Alvarez de Toledo et al., 1993; Lollike et al., 1998; Spruce et al., 1990). Beyond that critical threshold the pore expands irreversibly, in a manner that is consistent with full-fusion exocytosis. Fusion pore kinetics have been shown to be affected by both cytosolic and extracellular calcium concentrations (Ales et al., 1999; Hartmann and Lindau, 1995), activation of protein kinase-C (Scepek et al., 1998), and by interventions with proteins of the exocytotic machinery, such as complexin (Archer et al., 2002), synaptotagmin (Wang et al., 2001), and syntaxin (Han et al., 2004).

Parallel amperometric recordings of membrane capacitance and catecholamine release demonstrated that at least some transmitter molecules can leak through the initial fusion pore (Albillos et al., 1997; Alvarez de Toledo et al., 1993), albeit at a slow rate. This slow initial release through the fusion pore

gives rise to a characteristic pre-spike feature ('foot') in amperometric recordings, while bulk release of catecholamine coincides with the beginning of the final and irreversible expansion of the pore (Albillos et al., 1997; Alvarez de Toledo et al., 1993). However, these findings are difficult to interpret because charged transmitter molecules are bound to a gel-like matrix within the lumen of the granule (Uvnäs and Åborg, 1988), and hydration of this matrix is a prerequisite for bulk release of the bound molecules (Marszalek et al., 1997). In contrast to catecholamines, some proteins are initially retained in the granule despite an already open fusion pore (Barg et al., 2002; Perrais et al., 2004). In insulin-secreting cells, there is a delay of up to 10 seconds after pore formation, before the entire peptide contents is rapidly released [<100 milliseconds (Barg et al., 2002; Michael et al., 2004)] and large tracer molecules can enter the granule (Takahashi et al., 2002). Since this phenomenon is reminiscent of the bulk release of catecholamine that occurs at the moment of irreversible pore expansion, the latter findings suggest that peptides with a size similar to that of the fusion pore (2-3 nm) are unable to pass the initial fusion pore at a significant rate. Notably, the molecular dimensions of many of the peptide hormones are similar to estimates of the diameter of the transient fusion pore (Lindau and Almers, 1995).

These findings raise the question whether release is regulated beyond the moment of membrane fusion, and specifically whether a transient fusion mechanism may enable cells to release selectively low-molecular-weight transmitters from LDCVs. Here we have studied exocytosis and cargo discharge from individual LDCVs in Ins1-cells, a well-established model of neuroendocrine Ca^{2+}-dependent secretion (Asfari et al., 1992). Exocytosis was measured in three complementary ways. First, we monitored membrane fusion using high-resolution capacitance measurements, which reports the increase in cell surface area that occurs during exocytosis. Second, the release of nucleotides was studied at the single-vesicle level as nucleotide-activated currents measured in cells transfected with ionotropic purinergic receptors (Khakh et al., 2001). Third, peptide release and vesicle fusion were investigated in individual granules by real-time imaging of fluorescent reporter proteins and dyes. We report that up to two-thirds of exocytotic events were not associated with detectable peptide release but nevertheless resulted in the release of ATP. These data suggest that the release of peptides and low-molecular-weight granule constituents is differentially regulated following membrane fusion, possibly at the level of the fusion pore itself.

Materials and Methods

Culture and transfection of Ins1-cells

Ins1-cells (passages 85-106) were grown in RPMI 1640 medium (10 mM glucose; Gibco BRL) supplemented with 10% fetal bovine serum, streptomycin (100 μg/ml), penicillin (100 μg/ml), Na-pyruvate (1 mM), and 2-mercaptoethanol (50 μM). Cells were transfected using Fugene 6 (Roche) or Lipofectamine2000 (Invitrogen), according to the protocols recommended by the manufacturers. Following transfection, the cells were replated on glass coverslips and used within 3 days.

Solutions

During the electrophysiological and optical recordings the cells were constantly perfused with extracellular solution (EC) consisting of (in mM) 138 NaCl, 5.6 KCl, 1.2 $MgCl_2$, 2.6 $CaCl_2$, 1 D-glucose and 5 Hepes (pH 7.4 with NaOH). When exocytosis was elicited by voltage-clamp depolarizations, 20 mM of NaCl was equimolarly replaced with tetraethyl ammonium-chloride (TEA-Cl) to facilitate the detection of inward Ca^{2+}-currents. In Fig. 1C, $CaCl_2$ was increased to 10 mM. The pipette solution in the latter experiments (Figs 3-4) contained (in mM) 125 CsCl, 10 NaCl, 1 $MgCl_2$, 0.05 EGTA, 3 Mg-ATP, 0.1 cAMP, 5 Hepes (pH 7.15 using CsOH). In other experiments (Fig. 2B-D and Fig. 6), exocytosis was elicited by intracellular dialysis of the cell with a buffer containing (mM) 125 CsCl, 10 NaCl, 1 $MgCl_2$, 10 EGTA, 9 $CaCl_2$, 3 Mg-ATP, 0.1 cAMP, 5 Hepes (pH 7.15 using CsOH). The free Ca^{2+} concentration was calculated to be 2.0 μM (WinMaxChelator, http://www.stanford.edu/~cpatton/). All experiments on living cells were carried out at 32-34°C. Rapid local application of high K^+- or NH_4Cl-containing solutions was achieved with a Nanoliter 2000 injector (World Precision Instruments, Sarasota, FL).

Electrophysiology

Patch electrodes were pulled from borosilicate glass capillaries coated with Sylgard close to the tips and fire-polished. The pipette resistance ranged between 2 and 4 MΩ when filled with the

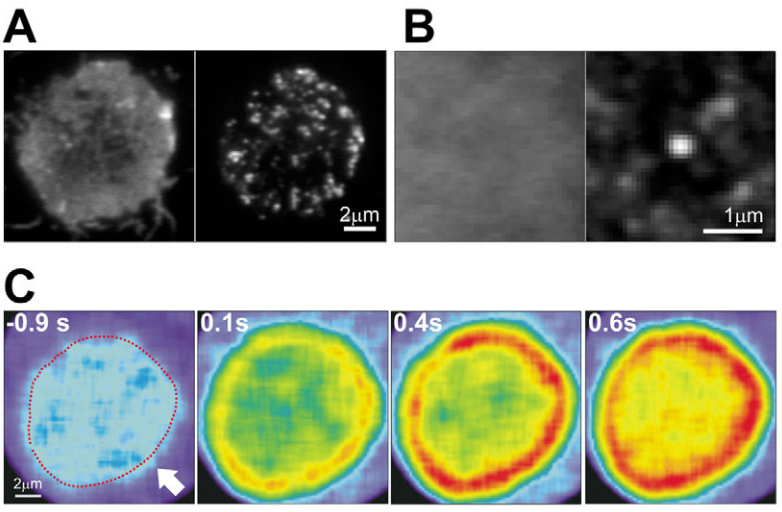

Fig. 1. (A) TIRF-images of a cell transfected with $P2X_2$-mRFP1 (left panel) and IAPP-EGFP (right panel). (B) Average image of 23 small frames taken from images like those shown in A and centered on the location of granules (right panel, IAPP-EGFP spots). The left panel is the average image of similar frames cut at the same locations from the red channel. Note uniform $P2X_2$-mRFP1 labeling (left). (C) Sequence of confocal images showing Fluo-5F fluorescence in a cell that expressed $P2X_2$-mRFP. At t=0 seconds, ATP (2 mM) was applied to the cell via a puffer pipette from the direction indicated with an arrow.

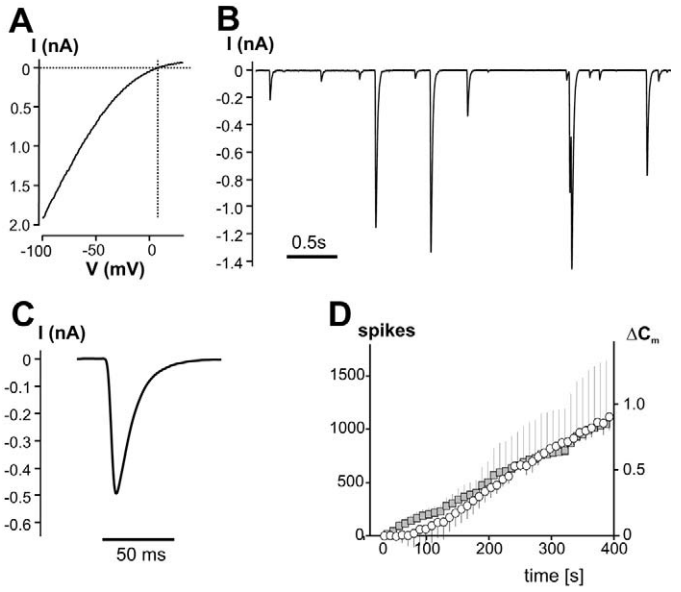

Fig. 2. Electrophysiological detection of nucleotide release from individual LDCVs. (A) Current (I)-voltage (V) relationship in a cell expressing $P2X_2$-EGFP. The current was activated by application of 0.2 mM ATP through a puffer pipette, and the I-V characteristics were then determined by ramping the membrane potential from –100 to +30 mV. The response obtained before application of ATP was subtracted from that recorded immediately after addition of the nucleotide to obtain the net current. The dotted horizontal and vertical lines represent the zero-current and the reversal potential, respectively. (B) Typical recording of current spikes evoked in a $P2X_2$-expressing cell by dialyzing the cell interior with a solution containing 2 μM free Ca^{2+}. (C) Current spike obtained by averaging 32 recorded events (black line) with an amplitude ranging between 400 and 600 pA. (D) Cumulative number of current spikes recorded in four cells as shown in Fig. 1C (gray squares) and increase in whole-cell capacitance recorded in parallel (open circles) measured at 0.1 Hz. The scaling corresponds to 0.8 fF per spike (MacDonald et al., 2005).

intracellular solution specified above. The measurements were conducted using an EPC-9 amplifier and the Pulse software (version 8.4 or later; Heka Elektronik, Lambrecht, Germany). Exocytosis was elicited by voltage-clamp depolarizations from –70 mV to zero and detected as changes in cell capacitance estimated by the 'Sine + DC'-feature of Pulse, using a 500 Hz, 20 mV sine. The experiments were performed in the whole-cell configuration with an access resistance of 10-20 MΩ. For membrane currents ⩽500 pA, the voltage error is limited to ~5 mV. In Fig. 2B,C and Fig. 3A,B, $P2X_2$-currents were filtered at 1.67 kHz and sampled at 5 kHz. Spike analysis was performed using MiniAnalysis software (Synaptosoft, Decatur, GA) setting the threshold at five times the RMS noise during event-free sections of the recordings (5-8 pA). Spikes in Fig. 3A were detected by eye. We point out that this assay provides information similar to that obtained by amperometry but that it has the advantage of detecting all release events in the entire cell whereas carbon fiber amperometry usually covers only a fraction of the cell.

Analysis of $P2X_2$ receptor distribution on the plasma membrane

It has previously been shown that the electrophysiological properties of $P2X_2$-EGFP are similar to those of unlabeled $P2X_2$ (Khakh et al., 2001). We ascertained uniform expression of the expressed $P2X_2$ receptors using total internal reflection microscopy (TIRF; see below). In Ins1-cells expressing $P2X_2$-mRFP1 (Fig. 1A,B, left panels) and the granule marker IAPP-EGFP (Fig. 1A,B, right panels), the fluorescence intensity of $P2X_2$-mRFP1 in the footprint of the cell exhibited a standard deviation of 31±2% (n=7 cells) of the background-subtracted mean. This level of variation is primarily due to uneven illumination, because it was seen also in cells stained with the membrane dye FM4-64 (standard deviation 28±1%; n=4; not shown). There was no evidence for preferential localization of $P2X_2$-mRFP1 with regard to individual granules, and when 23 small frames each with a granule in the center were averaged, the corresponding average image in the $P2X_2$-mRFP channel appeared even (Fig. 1B, left). In the individual frames, the mRFP1 signal within a 0.5 μm circle corresponding to the site of the granule (identified by IAPP-EGFP) was the same (103±2%; n=23) as that of a surrounding 2 μm-wide annulus.

To test whether the observed fluorescence distribution represents functional $P2X_2$-receptors, we took advantage of the fact that $P2X_2$ is somewhat permeable to Ca^{2+}, and imaged ATP-evoked Ca^{2+}-influx in cells that expressed $P2X_2$-mRFP. Cells were dialyzed in whole-cell voltage-clamp mode (–70 mV) with a solution containing (in mM) 120 Cs-glutamate, 10 CsCl, 10 NaCl, 1 $MgCl_2$, 10 Hepes, 3 Mg-ATP 10 EGTA and 0.2 Fluo-5F (Molecular Probes, Eugene, OR), adjusted to pH 7.15 using CsOH. The combination of low-affinity Ca^{2+}-indicator and high concentration of Ca^{2+}-chelator has previously been shown to resolve Ca^{2+}-microdomains (Zenisek et al., 2003). A central plane of the cell was then selected and imaged with a confocal microscope at 10 Hz (Fig. 1C). At time zero, 2 mM ATP (in EC with 10 mM $CaCl_2$) was applied through a local puffer pipette to activate $P2X_2$-channels. Immediately after ATP application, the Ca^{2+}-signal increased uniformly in a rim below the plasma membrane of the cell (Fig. 1C), indicating uniform expression of functional $P2X_2$-channels. The lesser increase in the Ca^{2+}-indicator signal at the upper left corner was seen in all cells and is likely due to the larger distance from the mouth of the ATP-puffer pipette (direction of puff indicated with an arrow in Fig. 1C).

Live cell imaging

The images in Fig. 1A-B were obtained with a custom-built lens-type total internal reflection fluorescence (TIRF) microscope equipped with a 100×/1.65 Apo lens (Olympus, Melville, NY). The 488 nm line of an Argon/Krypton laser (Innova 70C, Coherent, Santa Clara, CA) was used to excite both EGFP and mRFP1, and their emission was imaged simultaneously with an image splitter (Multispec MicroImager, Optical Insights, Santa Fe, NM) that separated the red and green components into two channels as side-by-side images on the chip of a charge-coupled device (CCD) camera (Cascade 512B, Roper Scientific, Trenton, NJ). The final spacing was 80 nm per pixel. A lens (400 mm focal length) was included in the emission path of the red channel to correct for a slight focus difference between the red and green channels. To correct for any residual mis-registration and differences in magnification caused by the lens, we acquired pictures of scattered 200 nm beads (Molecular Probes, Eugene, OR) fluorescing at both wavelengths. Beads in the two images were brought into superposition by shifting, stretching, or shrinking the image of the red channel with in-house software (Taraska et al., 2003) written in Matlab (Mathworks, Natick, MA). The parameters thus obtained were used to correct the cell images and resulted in a shift of 5 pixels or less. All images were acquired with MetaMorph software (Universal Imaging, Downingtown, PA).

All other images were obtained on inverted scanning confocal microscopes (LSM510 or Pascal, Carl Zeiss, Jena, Germany). Fluo-5F, EGFP, pHluorin and EMD were excited with the 488 nm argon line and emission was collected through a 100×/1.4 NA objective at >505 nm or 505-530 nm (Fig. 7). The theoretical optical resolution

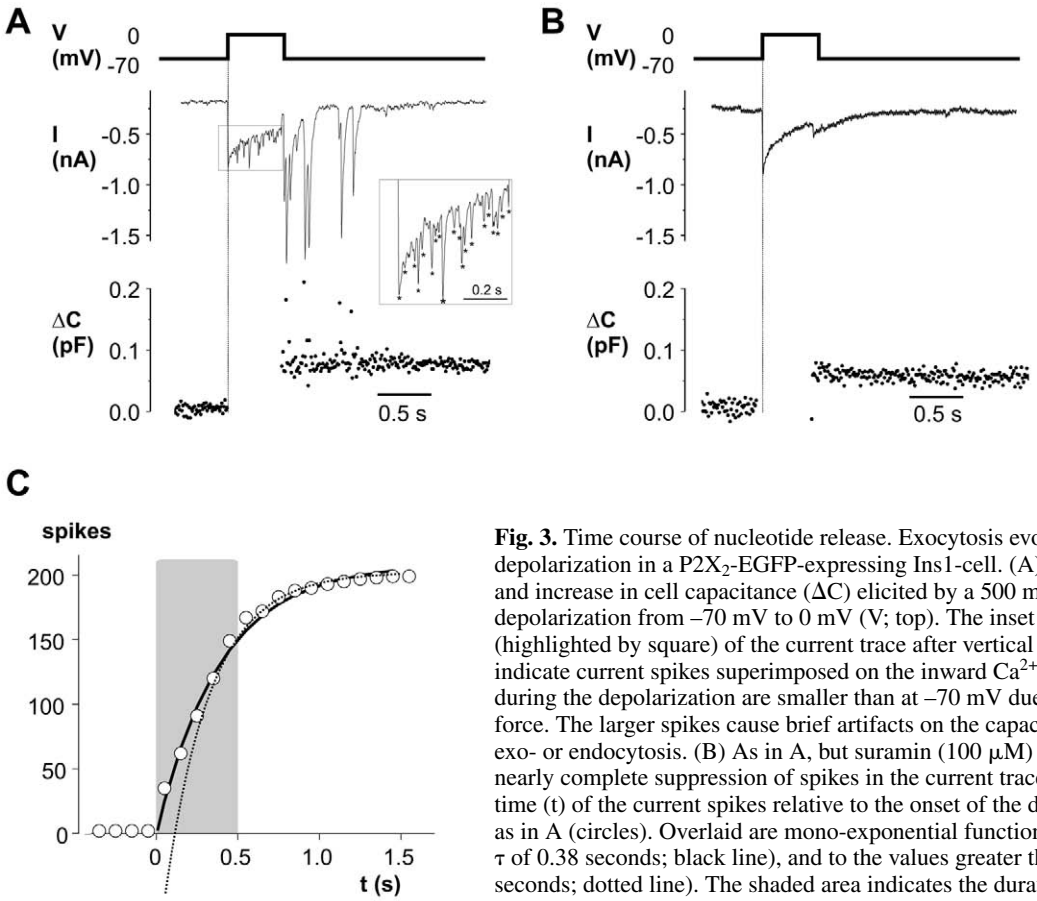

Fig. 3. Time course of nucleotide release. Exocytosis evoked by voltage-clamp depolarization in a $P2X_2$-EGFP-expressing Ins1-cell. (A) Membrane currents (I; middle) and increase in cell capacitance (ΔC) elicited by a 500 millisecond voltage-clamp depolarization from –70 mV to 0 mV (V; top). The inset shows the indicated part (highlighted by square) of the current trace after vertical and horizontal expansion. Asterisks indicate current spikes superimposed on the inward Ca^{2+}-current (identified by eye). Spikes during the depolarization are smaller than at –70 mV due to the reduced inward driving force. The larger spikes cause brief artifacts on the capacitance trace that are unrelated to exo- or endocytosis. (B) As in A, but suramin (100 μM) was applied to the cell, resulting in nearly complete suppression of spikes in the current trace. (C) Cumulative histogram of the time (t) of the current spikes relative to the onset of the depolarization in eleven experiments as in A (circles). Overlaid are mono-exponential functions fitted to all points (time constant τ of 0.38 seconds; black line), and to the values greater than 500 milliseconds (τ of 0.28 seconds; dotted line). The shaded area indicates the duration of the depolarizing stimulus.

with this configuration is 213 nm (Abbe's criterion), and we scanned at 0.12 μm/pixel (Figs 4-6), 0.6 μm/pixel (Fig. 7C,D) or 0.18 μm/pixel (Fig. 1C). In the experiment shown in Fig. 5, ECFP was excited at 458 nm and detected at 465-495 nm on the forward scan. On the return scan of each line, pHluorin was excited at 514 nm and detected at <560 nm. The scan speed was 1.5 milliseconds per line pair. At the settings used, 19±5% (n=16) of the signal in the pHluorin channel crosstalks into the ECFP channel. The bottom layer of granules (referred to as the footprint of the cell) was found by moving the focal plane upwards from below the cell towards the plane with the maximum intensity of the first appearing granules. For display purposes, the images shown in Fig. 5 have been averaged over four consecutive frames.

In Fig. 6, electrophysiological detection of ATP release was combined with simultaneous optical detection of IAPP-pHluorin in the entire cell. We employed a 40×/1.25W objective, the plane of focus was set in the center of the cell, and the axial resolution was reduced by opening the confocal pinhole to its maximum setting. The measured point-spread function in this configuration has an axial width of 7.3 μm at half-maximum, comparable with the height of Ins1-cells adhering to the coverslip (Barg et al., 2002). Electrophysiology and imaging were synchronized by trigger signals generated by the Pulse software or (in Fig. 6) the confocal microscope.

Image analysis

LDCVs undergoing exocytosis were detected manually by repeatedly playing the movies fast forward and reverse. The fluorescence intensity was then determined by defining a circular region-of-interest (ROI) of about 0.5 μm diameter at the spot where an event occurred. The data are displayed either as the mean of the ROI (8-bit resolution) divided by the initial fluorescence (F/F_0; for EGFP, EMD and ECFP), or divided by the peak fluorescence (F/F_{peak}; for pHluorin). In Fig. 6A,B local background was measured in an area close to the granule and subtracted from the raw data. In Fig. 6C,D, a ROI was defined around the entire cell (see Fig. 6C,D, white line) and corrected by the average value of a background ROI defined outside the cell, for each frame.

Dextran uptake

For uptake experiments, Ins1-cells plated on coverslips were first incubated in standard EC (see Solutions) at 34°C for 30 minutes. Exocytosis was then stimulated using a buffer containing (mM) 83.6 NaCl, 60 KCl, 1.2 $MgCl_2$, 2.6 $CaCl_2$, 5 HEPES (adjusted to pH 7.4 with NaOH), 1 glucose, and 14 μM Alexa568-hydrazine (Molecular Probes, Eugene, OR) for 30 seconds. The cells were then washed five times with ice-cold EC before fixation in formaldehyde (3%). Cells were imaged using a confocal microscope as described above. Random co-localization was estimated as 7% in image pairs in which the two channels had been brought out of register by rotation and/or mirroring. It was ascertained by imaging neighboring planes that co-localized vesicles were spherical and located in the same plane.

Statistical evaluation

Data are quoted as the mean values ±s.e.m. of indicated number of experiments or cells as indicated. Non-linear fitting was done in Origin (OriginLab, Northampton, MA, USA). Statistical significances were evaluated using Student's t-test.

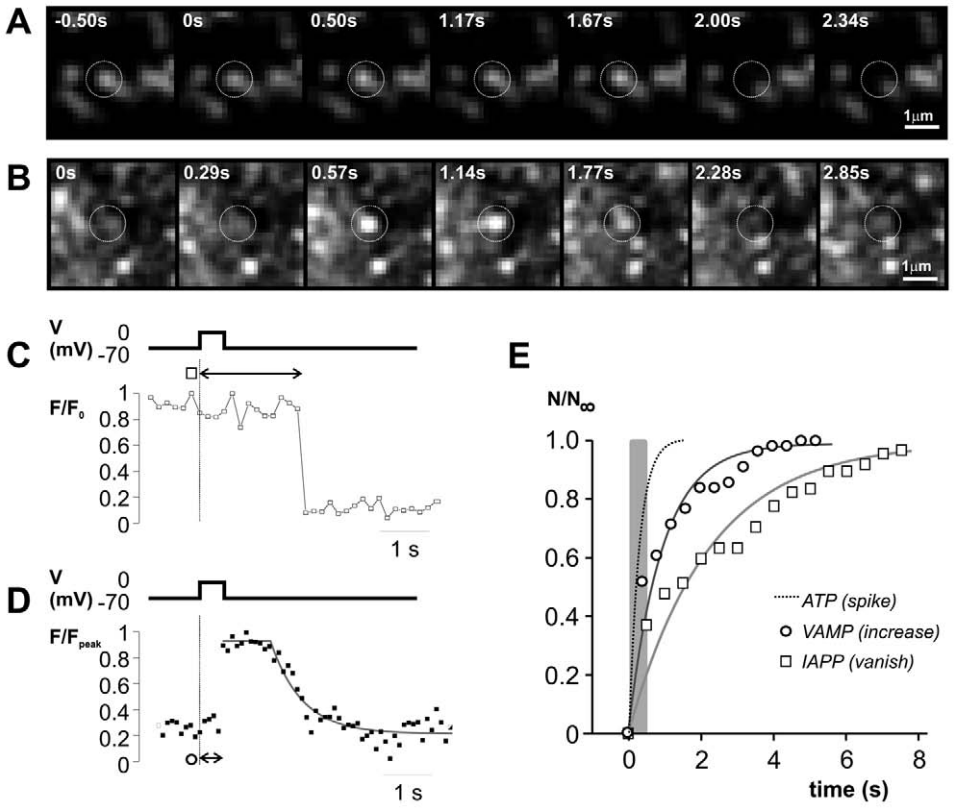

Fig. 4. Time course of peptide release and luminal pH changes. (A,B) Cells expressing VAMP-pHluorin or IAPP-emerald (IAPP-EMD) were voltage-clamped and their footprint imaged at 10 Hz. Example images taken in separate cells transfected with IAPP-EMD (A) or VAMP-pHluorin (B) at the indicated times relative to the onset of a 500 millisecond depolarization from –70 mV to zero mV. (C) Time course of IAPP-EMD fluorescence (lower trace) in the ROI indicated by the circle in A in response to a 500 millisecond depolarization (top trace). Note that the IAPP-EMD fluorescence disappears after a delay of ≈2 seconds. (D) As in C for the experiment shown in B. Note that the VAMP-pHluorin trace rises abruptly to a plateau from which it declines mono-exponentially after a delay of ≈1 second. The gray line superimposed on the data points represents the best fit of a discontinuous function consisting of a straight-line segment followed by a mono-exponential decay to the remainder of the trace, using the first point of the rising phase as the start of the event. (E) Cumulative histograms showing the time, relative to stimulation, of the loss of IAPP-EMD fluorescence (squares), the increase in VAMP-pHluorin fluorescence (circles) analyzed as indicated by arrows in C and D. The functions superimposed on histograms in E are exponential functions fitted to the distributions yielding τ-values of 0.9±0.1 (circles), and 2.2±0.2 seconds (squares). For comparison, the function from Fig. 3B (fit to the nucleotide release data >500 milliseconds) is included as a dotted line.

Results

Release of adenine nucleotides from insulin-containing LDCVs

To investigate the time course of nucleotide release from LDCVs we transfected GFP-labeled purinergic receptors ($P2X_2$-GFP or $P2X_2$-mRFP1 (Khakh et al., 2001), into clonal Ins1-cells. In these cells, release of adenine nucleotides from LDCV will evoke 'autaptic' activation of the expressed $P2X_2$-channels and give rise to transient inward whole-cell currents similar to the excitatory postsynaptic currents (EPSCs) that can be recorded from neurons. It was ascertained that functional $P2X_2$-receptors were uniformly expressed in the plasma membrane (Fig. 1A-C) (see Materials and Methods for details). Cells expressing $P2X_2$-EGFP were then voltage-clamped at –70 mV and the receptors activated by brief exposure to 0.2 mM ATP. The application of ATP evoked large and rapidly activating inward currents with an average magnitude of 3.2±0.4 nA (n=13, not shown). Voltage ramps from –100 to +30 mV during the application of ATP confirmed that the $P2X_2$ currents exhibited strong inward rectification and the current amplitude at zero mV was only 6±3% (n=8) of that seen at –70 mV (Fig. 2A).

We elicited exocytosis in cells expressing $P2X_2$-EGFP by dialyzing the cytosol with a pipette solution containing 2 μM free Ca^{2+}, while holding the membrane potential at –70 mV. Shortly after formation of the whole-cell configuration, inward current spikes were observed (Fig. 2B,C). Of the 1640 events recorded, 559 were single spikes were sufficiently separated from neighboring spikes to allow more detailed analysis. On average, these spikes reached a peak amplitude of 500±30 pA, had a rise time (10-90%) of 5.0±0.1 milliseconds, deactivated mono-exponentially with a time constant of 16±1 milliseconds and carried an average charge of 10±1 pC. A pre-spike feature, reminiscent of the 'foot' described in amperometric recordings from chromaffin cells (Chow et al., 1992), was observed in only 3% of the events (not shown). We repeated the experiment and recorded the increase in whole-cell membrane capacitance in parallel (Fig.

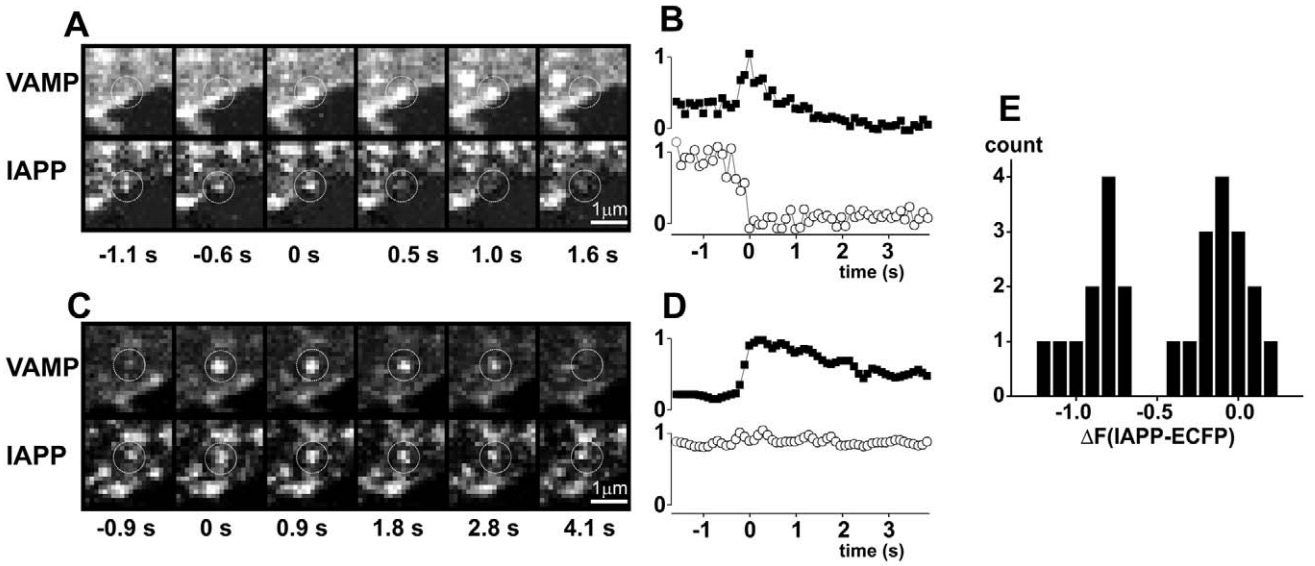

Fig. 5. Exocytosis does not necessarily lead to peptide release. (A,C) Simultaneous imaging of VAMP-pHluorin (top) and IAPP-ECFP (lower) in double-transfected cells. The cell (imaged at 10 Hz) was stimulated with a 3 second puff of solution containing 87 mM KCl. Times quoted below the images are relative to the peak in the VAMP-pHluorin signal. (A) Example of a granule (highlighted by a circle) that showed a transient increase in VAMP-pHluorin fluorescence and that culminated in the loss of IAPP-ECFP fluorescence. (B) Fluorescence intensities of IAPP-ECFP (open circles) and VAMP-pHluorin (black squares) within ROIs centered on the granule highlighted in A. (C) Example where the increase in VAMP-pHluorin fluorescence was not associated with the rapid loss of IAPP-ECFP fluorescence. (D) As in B, but for the granule shown in C. (E) Analysis of IAPP-ECFP fluorescence in 28 cells and in A,C. Data in the histogram were derived from traces as in B and D by subtracting the intensity measured at t=5.25 seconds from that at –1.0 second, both averaged over 0.5 second.

2D). In four separate experiments, a mean of 1000±541 spikes was observed during the first 400 seconds, and the associated capacitance increase was 895±87 fF. From these values, we estimate the unitary capacitance increase to be ~0.9 fF/spike assuming that endocytosis is negligible under these experimental conditions. However, no capacitance increase occurred during the first ~50 seconds, while spiking happened at about the same frequency during the entire 400 s. This finding is consistent with endocytosis taking place mainly during the first minute of the recoding, before necessary cytosolic factors may have been washed out. To avoid this effect, regression lines were fit to the data between 100 and 400 seconds, which yielded slopes of 2.62 fF per second for the capacitance increase, and 2.65 spikes per second for the $P2X_2$-currents. With these values the unitary capacitance increase calculates to 1.0 fF per spike, in reasonable agreement with the 0.8 fF obtained by high-resolution cell-attached capacitance (MacDonald et al., 2005). In conclusion, expression of $P2X_2$ in the cell of interest allows reliable detection of nucleotide release from single granules, with millisecond time resolution.

Time course of nucleotide release

We exploited the $P2X_2$ receptor-based assay to determine the time course of nucleotide release in response to a single voltage-clamp depolarization. Ins-1 cells are well suited for this type of stimulus because exocytosis is tightly coupled to Ca^{2+}-influx and essentially limited to the duration of the stimulus (Barg et al., 2002; Yang et al., 2002). We recorded membrane capacitance and currents in cells expressing $P2X_2$-EGFP, and applied a single depolarization lasting 500 milliseconds. In the experiment shown in Fig. 3A, the observed capacitance increase of 70 fF was confined to the duration of the depolarization and no further increase occurred after the voltage was stepped back to –70 mV. This corresponds to the release of 88 granules using a conversion factor of 0.8 fF per granule (MacDonald et al., 2005). In parallel, we detected a series of transient inward currents that resembled the spikes observed during intracellular Ca^{2+} infusion (cf. Fig. 2B). As shown by the inset, numerous current spikes (highlighted by asterisks) were superimposed on the Ca^{2+}-current and continued for ~1 seconds after the end of the stimulation. In this experiment, 12 events were observed while there was no further increase in cell capacitance. As expected from the current-voltage relationship of the ATP-gated current (Fig. 2A), the spikes observed at –70 mV were ≈20-fold larger than those seen during the depolarization. Inclusion of the purinergic antagonist suramin (100 μM) in the extracellular solution had no effect on the capacitance increase but almost abolished the current spikes (Fig. 3B), confirming that they result from activation of purinergic receptors. In a series of ten experiments as in Fig. 3A, a total of 199 current spikes were detected, 50 of which occurred after the end of the depolarization. The histogram in Fig. 3C shows the cumulative latency histogram of these events, measured from the onset of the depolarization to the peak of the spike. Approximating a single exponential function to the data suggests that ATP is released with a time constant (τ) of 385 milliseconds, which is ~4-fold slower than the time course of capacitance increase (Barg et al., 2002). However, because not all current spikes can be resolved during the depolarization, this value is likely

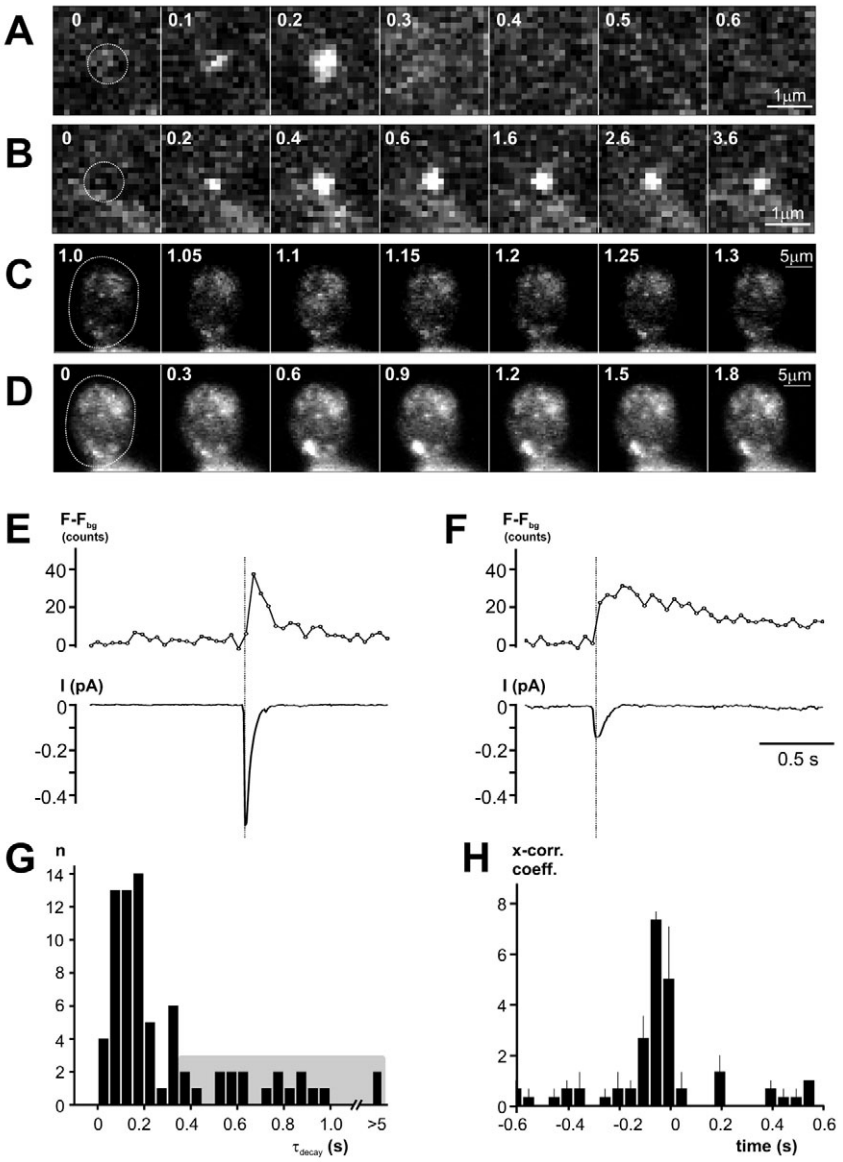

Fig. 6. Parallel recording of nucleotide and peptide release from individual granules. (A,B) Confocal images of a section of the footprint of a voltage-clamped cell expressing both IAPP-pHluorin and P2X$_2$-mRFP. The images were recorded at the indicated times relative the onset of the IAPP-pHluorin flash. Exocytosis was elicited by intracellular dialysis of the cell with a buffer in which $[Ca^{2+}]_i$ was set at 2 μM. Note that the highlighted granules increase their fluorescence during the displayed sequence. In A, the signal from the granule is rapidly lost, while in B it remains elevated for several seconds. (C,D) Image sequences of a cell co-transfected with IAPP-pHluorin and P2X$_2$-mRFP1 and stimulated as in A and B. The entire cell was imaged in the IAPP-pHluorin channel (see Materials and Methods), and whole-cell current spikes due to activation of the P2X$_2$ receptors were recorded in parallel. Examples of a short-lived fluorescence transient in C, and a long-lasting event in D. (E,F) Time course of the average fluorescence intensity in the ROIs indicated by the white circle in C and D (top) and inward membrane currents associated with the events (lower). Note slow decay of fluorescence in F. (G) Histogram of the decay constants of 56 events as in C and D. The shaded area indicates decay constants greater than 350 milliseconds. (H) Cross-correlation histogram of the times of fluorescence peaks vs the times of current peaks in three experiments similar to that shown in C and D.

underestimating the true rate of nucleotide release. When the fit was instead limited to only the 50 events observed after the pulse, when they could reliably be resolved, a τ of 280 milliseconds was derived (dotted line in Fig. 3C). In the latter case, the fitted curve extends below the ordinate, as expected if many events escaped detection. Both time constants are longer than that for the capacitance increase and we conclude that release of adenine nucleotides lags slightly (<200 milliseconds) behind membrane fusion.

Time course of peptide release

We next monitored the time course of peptide release from Ins-1 cells using chimeric constructs of IAPP with various fluorescent proteins. These constructs result in soluble proteins that are correctly targeted to the granule lumen (Barg et al., 2002; Michael et al., 2004). To monitor the time course of peptide release without interference of granular pH changes, we tagged IAPP with the essentially pH-insensitive fluorescent protein emerald (EMD) (Tsien, 1998). Cells expressing IAPP-EMD were imaged in a plane adjacent to the coverslip with a confocal microscope and simultaneously voltage-clamped. We then applied the same single 500 millisecond depolarization stimulus as in Fig. 3, which resulted in the sudden loss of fluorescence from several IAPP-EMD labeled granules. Fig. 4A shows part of a cell where such an event occurred (granule highlighted by the circle). As illustrated in Fig. 4C, the fluorescence in the example of Fig. 4A was initially stable and then disappeared about 2 seconds after the onset of the stimulus. Vertical movement of the granule out of the focal plane is unlikely to account for the disappearance of fluorescence because the granule vanished within <100 milliseconds. The axial resolution of the microscope in these experiments was ~0.8 μm (estimated from the half-width at 10% intensity of the point-spread function). This suggests that the granules would have to move out of focus at speeds >8 μm per second to allow the fluorescence signal to decay by ⩾90%. This is almost ten-fold the maximum horizontal speed actually

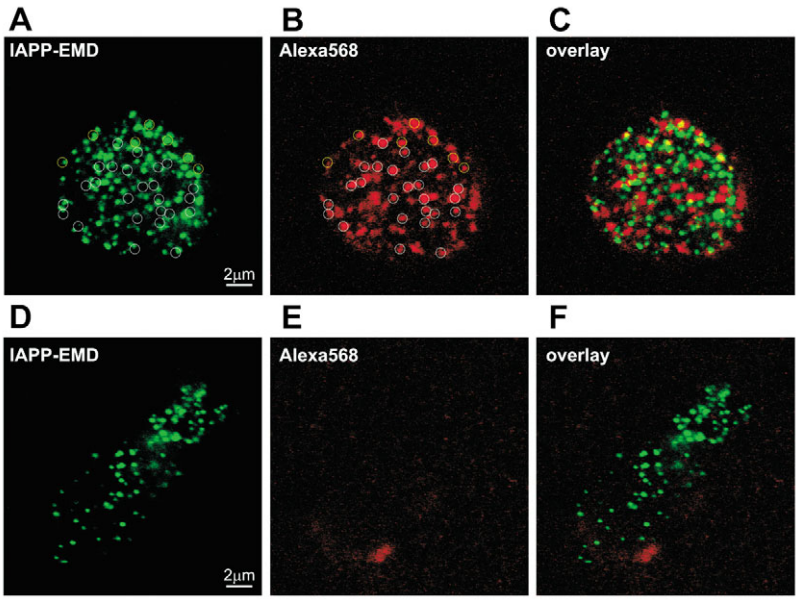

Fig. 7. Stimulation-dependent uptake of endocytotic tracer dye. (A-C) Uptake of Alexa563-hydrazine (red; B) in cells expressing IAPP-emerald (green; A). Vesicles containing only Alexa563-hydrazine are highlighted by white circles, and vesicles containing both labels are highlighted by yellow circles and appear yellow when the images are merged, as shown in C. Exocytosis was stimulated for 30 seconds with 87 mM KCl, followed by washing on ice. (D-F) As in A-C, but the cells were incubated in standard EC solution (5 mM KCl) containing Alexa563-hydrazine.

observed in these cells (<1 μm per second) (Ivarsson et al., 2004). From records such as in Fig. 4C we determined the time of fluorescence loss, relative to the onset of the depolarization. The data are plotted in a cumulative histogram in Fig. 4E and can be described by an exponential function with a time constant τ=2.2±0.2 seconds. This is similar to the value we reported previously for the release of IAPP-EGFP (Barg et al., 2002) and ~6-fold slower than the time constant for nucleotide release determined above (dotted line).

Time course of granule pH-equilibration

Mature granules have a luminal pH of ~5.5 that equilibrates during exocytosis with the extracellular pH. We took advantage of this feature to monitor granule fusion, by using the pH-sensitive fluorescent protein pHluorin fused to the luminal side of VAMP-2 (VAMP-pHluorin) (Miesenbock et al., 1998). In insulin-secreting cells, both endogenous VAMP and VAMP-EGFP are principally localized to granules (Regazzi et al., 1995; Tsuboi et al., 2004). We tested for co-localization in double-transfected Ins1-cells and found that 88±2% of the VAMP-pHluorin-positive vesicles also contained the granule-specific marker IAPP-mRFP1 (n=288 in 6 cells; data not shown). We also tested the effect of elevating the luminal pH on VAMP-pHluorin fluorescence. Bath application of NH_4Cl (50 mM) resulted in an 11±2-fold increase in the fluorescence of VAMP-pHluorin-labeled granules (n=26 vesicle from 6 cells; not shown).

A similar increase in granule fluorescence is expected during exocytosis and should indicate fusion pore opening. We again imaged cells and subjected them to a single voltage-clamp depolarization, as in Fig. 4A. During and after the stimulus, several fluorescent puncta appeared throughout the cell. Fig. 4B shows an area of a cell in which such an event occurred (highlighted by a circle) and the dotted trace in Fig. 4D shows the mean fluorescence intensity within the circle indicated in Fig. 4B. The fluorescence in the spot suddenly increased at the end of the stimulus, stayed bright for another second and then decayed back to baseline. The initial rise occurred within a single frame (0.1 second). As discussed above, this is too quick to be accounted for by vertical granule movement. Contrary to what would be expected if the granule had collapsed into the plasma membrane, 39 of the granules (70%) retained more than two-thirds of their peak fluorescence one second after exocytosis. This confirms the previous finding in PC12 and Min6 cells that the granule stays morphologically intact at least temporally following exocytosis (Taraska et al., 2003; Tsuboi et al., 2004).

We quantified traces as in Fig. 4D by determining (1) the latency of the fluorescence increase relative to the stimulus (illustrated with an arrow in Fig. 4D), (2) the duration of the plateau period, and (3) the time constant of an exponential fit to the decay phase. The cumulative distribution of the latency for a total of 56 events (21 cells) is shown in Fig. 4E. The distribution increases monophasic and a single exponential fit yielded a time constant of τ=0.9±0.1 seconds, which is intermediate between that of ATP release (<0.35) and peptide release (2.2 seconds) (Fig. 4A,C,D). The fluorescence remained then elevated for an average of 1.0±0.2 seconds (plateau phase), and the final decay phase had an average time constant of τ=7.1±2.3 seconds (median 1.95 seconds). The rapid increase in fluorescence during the stimulus indicates that VAMP-pHluorin is a useful probe of exocytotic fusion. However, the decay phase is more ambiguous and may be caused either by pore closure and reacidification of the granule (Taraska and Almers, 2004) or by the escape of VAMP-pHluorin into the plasma membrane (Tsuboi and Rutter, 2003).

Exocytosis without release of peptides

Since it is possible to detect both fusion pore opening and peptide release with fluorescent probes (Fig. 4), we next asked whether pore opening is always associated with peptide release. In these experiments, we co-transfected cells with VAMP-pHluorin and IAPP fused to the pH-insensitive enhanced cyan fluorescent protein (IAPP-ECFP). The cells

were imaged simultaneously in the ECFP and pHluorin channels and stimulated by local application of KCl (87 mM). A total of 32 exocytotic events (detected as transient increases in the pHluorin channel) were observed in 12 cells. In some of these events, the increase in pHluorin fluorescence was clearly associated with the abrupt disappearance of fluorescence from the corresponding spot in the IAPP-ECFP channel. An example is shown in Fig. 5A (granule highlighted with a circle), and Fig. 5B shows the associated fluorescence intensities in both channels for this granule. It can be seen that the IAPP-ECFP fluorescence vanished in <0.3 seconds and at the same time as the increase in VAMP-pHluorin. In other cases, the increase in pHluorin fluorescence occurred without concomitant decrease in ECFP-fluorescence. An example of such a granule is shown in Fig. 5C,D. The VAMP-pHluorin signal reached a peak within a fraction of a second, and then decayed slowly towards the original level. No significant change was detected in the IAPP-ECFP channel. We then quantified for the amount of IAPP-ECFP that was released by subtracting the granular ECFP-fluorescence immediately before the VAMP-pHluorin spike from that 5 seconds after the spike, both averaged over 0.5 seconds. In this analysis a value of zero corresponds to no release, and a value of –1 reflects complete release of IAPP-ECFP. The histogram of the 28 events that could be analyzed in this way (Fig. 5E) shows two clearly separated peaks, indicating that there was either complete release (peak around –1) or no release at all (peak around zero). This finding justifies grouping the data into eleven (39%) 'release' granules and seventeen (61%) 'no release' granules, and we conclude that in nearly two-thirds of the cases, exocytosis did not result in peptide release.

Nucleotide release is independent of peptide release

We have found that the luminal pH can equilibrate during exocytosis without peptide release (Fig. 5), and that release of nucleotides is at least as fast as pH-equilibration (Fig. 4). By analogy, this makes it plausible that nucleotides could be selectively released from granules that retain their peptide contents during an exocytotic event. To test this possibility, we combined the electrophysiological detection of nucleotide release with $P2X_2$ and the optical detection of exocytosis and release. For the latter, we used IAPP-pHluorin as probe, which combines the advantages of being sensitive to the pH-change after pore opening and being a soluble peptide that is potentially released from the granule.

It was first ascertained that the IAPP-pHluorin reports exocytosis. We imaged the footprint of cells expressing both IAPP-pHluorin and $P2X_2$-mRFP. The cells were then voltage-clamped at –70 mV and exocytosis was evoked by dialyzing the cell interior through the patch pipette with a solution containing 2 μM free Ca^{2+}. Soon after establishing the whole cell configuration, discrete spots of transient increases in fluorescence were observed. The events could be classified into two classes. In the first type of events (52%), there was a rapid loss of fluorescence that often coincided with the appearance of a short-lived cloud of fluorescence centered at the original spot (Fig. 6A). In the second type, the fluorescence remained elevated for several seconds and then slowly decayed towards the baseline (Fig. 6B). We defined fluorescence increases that decayed with time constants (τ) of <350 milliseconds and >350 milliseconds as rapid and persistent events, respectively. The average time constants of the rapid and persistent events thus classified were 0.12±0.02 seconds (median 0.09 seconds; n=14 events from four cells) and 7.3±2.0 seconds (median 5.0 seconds; n=13 events). Based on the rapid decay and the association with a cloud of fluorescence (Fig. 6A, fourth frame) it seems plausible to interpret rapid events as release of IAPP-pHluorin. The persistent events are consistent with granules that retain IAPP-pHluorin after exocytosis and dim slowly because of a combination of bleaching and re-acidification.

Next, we correlated the optical measurements of IAPP-pHluorin release with electrophysiological detection of nucleotide release. Since the latter method is insensitive to the location of release events, we adapted the microscope to allow detection of fluorescence emanating from the entire cell (see Materials and Methods). When the experiment was repeated with these microscope settings, transient fluorescence increases could be still be observed. Fig. 6C,D shows examples of two such events; note that an entire cell is displayed. Events could not be reliably detected by eye in these movies, and we therefore plotted the average intensity of the entire cell (circled with a white line). Fig. 6E,F shows the fluorescence intensity for the events shown in C and D. Single exocytotic events can thus be resolved optically even at the level of an entire cell. From these traces we calculated the decay constants of all detected events, and plotted them in the histogram shown in Fig. 6G. It can be seen that 19 out of 75 events (28±6%, n=3 cells) had decay constants >350 milliseconds (mean value: 0.66±0.05 seconds; median 0.75 seconds) whereas the remaining 56 (72%) events had a time constant <350 milliseconds (mean value: 0.16±0.01 seconds; median 0.15 seconds).

At the same time we detected transient ATP-activated currents in these cells (Fig. 6E,F, lower), similar to those in Fig. 2B. We determined the time of every peak in the fluorescence and current traces, and stored them in separate event lists. Cross-correlation analysis (Fig. 6H) of the event lists revealed a distinct peak at –50 milliseconds, indicating that the peak of the IAPP-pHluorin fluorescence lagged behind that of the current spikes. This confirms the earlier observation that pH-equilibration during exocytosis is somewhat slower than nucleotide release (Fig. 4). To determine how many of the current spikes were associated with a fluorescence event, we scored events as coinciding when the two peaks occurred within 0.4 seconds of each other. This analysis reveales that 68±14% of the current spikes were associated with either transient or persistent changes in fluorescence. This indicates that we detect release of ATP from granules, rather than other types of secretory vesicles. The lack of complete correlation is expected because in transiently transfected cells, not all granules will contain IAPP-pHluorin. For example, 24 hours after transfection, ~30% of LDCVs identified by immunostaining for phogrin do not contain IAPP-EMD (not shown). However, the 52 granules for which exocytosis could be detected with both methods were not different from the entire sample of 75 granules, and the ratio of rapid events (71%, τ=0.15±0.01 seconds) and persistent events (29±5%, τ=0.65±0.06 seconds) was similar. We conclude that nucleotide release occurs during both rapid (72%) and persistent events (28%), the latter of which we interpret as absence of peptide release.

Uptake of fluid phase tracer during exocytosis

Our data indicate that membrane fusion is not obligatorily associated with peptide release, and that some granules retain soluble peptides during exocytosis. We therefore tested whether such granules are able to reseal after exocytosis. To this end, we measured the vesicular uptake of the fluid phase marker Alexa568 (M_r 0.7, comparable with the M_r 0.5 for ATP) into cells expressing IAPP-EMD (Fig. 7A-F). Following stimulation with 87 mM external K^+ for 30 seconds, Alexa568 was rapidly taken up by into vesicles that were similar to IAPP-EMD labeled granules in apparent size and shape (Fig. 7B). Stained vesicles were confined to the rim just underneath the plasma membrane (not shown). Notably, 27±2% (n=10 cells) of all Alexa568-labeled vesicles also contained IAPP-EMD (Fig. 7C), indicating that these granules had undergone exocytosis without releasing (all of) the peptide marker. In control experiments, no uptake of Alexa-568 was detected in cells incubated in the same conditions but in a solution containing only 5 mM K^+ (Fig. 7D-F). Since labeling of granules with Alexa568 was resistant to extensive washing before fixation of the cells, we conclude that stained granules were no longer connected with the extracellular space.

Discussion

Differential release of small molecules and peptides

We have studied the time courses of membrane fusion, pH equilibration of the granule lumen, release of low-molecular-weight granule constituents and the exit of the peptide cargo associated with exocytosis in rat insulin-secreting Ins1-cells. Exocytosis in B-cells is initiated with a delay as short as 5-10 milliseconds after Ca^{2+}-influx (Barg et al., 2001). However, two key observations suggest that membrane fusion should not automatically be equated to instant and complete discharge of the secretory products. First, release is delayed relative to fusion of the granule with the plasmalemma. We found that release of adenine nucleotides was delayed by 0.1-0.2 seconds with respect to membrane fusion, and ATP-dependent current spikes were observed even after the capacitance had ceased to increase (Fig. 3A,C). A similar latency has been observed for serotonin release from insulin granules in experiments combining capacitance measurements and amperometry (Smith et al., 1999). Peptide release was delayed even further (~2 seconds on average) (Fig. 4A,C,E), consistent with our earlier study (Barg et al., 2002). Second, many granules stay structurally intact beyond the moment of fusion and the peptide cargo often remains within the granule after exocytosis (up to 70%, Fig. 5), confirming similar observations in neuroendocrine cells (Angleson et al., 1999; Holroyd et al., 2002; Perrais et al., 2004). In addition, we demonstrated here that nucleotides are released during exocytosis regardless of whether peptides are retained or not (Fig. 6). Taken together the data indicate that exocytosis of insulin granules can take two functionally different routes following membrane fusion: either complete emptying of the granule content, or selective release of only ions and small-molecular-weight compounds with (at most) partial release of the peptides.

Storage and release of nucleotides

Amperometric current spikes from mast- and chromaffin cells frequently (50-70%) have a pre-spike feature (‘foot’) that is believed to result from slow release of catecholamine or serotonin through the initial fusion pore (Chow et al., 1992). Although in our experiments the $P2X_2$ receptors were uniformly distributed (Fig. 1) and thus likely to be situated in the immediate vicinity of the release sites, such pre-spike features were rarely (3%) seen. We speculate that the apparent absence of a foot results from differences in the chemical characteristics of amines and adenine nucleotides rather than differences in their size. While adenine nucleotides have a more extended molecular structure (diameter 0.9-1.5 nm) than catecholamine (<1 nm in all dimensions), efflux of these molecules is unlikely to be limited by the initial fusion pore (2-3 nm). We rather attribute the absence of a ‘foot’ to the nature of the storage of ATP in the granule. Charged transmitter molecules like ATP bind to a polyanionic matrix within the granule (Nanavati and Fernandez, 1993; Uvnäs and Åborg, 1988; Verdugo, 1991), which could prevent their release at least during the life time of the initial fusion pore. It is well established that the granule matrix of chromaffin and other cells contains chromogranins and charged proteoglycans (Kiang et al., 1982). Other proteins may be involved as well, and the luminal domain of the synaptic vesicle membrane protein SV2 has been shown to be part of the matrix of synaptic vesicles (Reigada et al., 2003). The granule matrix acts like an ion exchange resin where liberation of the bound transmitter molecules requires influx of ions into the granule lumen to replace the charged transmitter molecules (Marszalek et al., 1997; Nanavati and Fernandez, 1993; Uvnäs and Åborg, 1988; Verdugo, 1991). Such a mechanism would result in a post-fusion modulation of release, and could account for the delay in ATP release. The absence of a foot signal may therefore indicate that ATP is discharged through an already expanded fusion pore.

Delayed peptide release

We show that the delay between fusion pore opening and peptide release is on average 2.2 seconds (Fig. 4A,C,E). It is not immediately evident why peptide release is even slower than ATP release but the bulkier nature of the peptide represents a possible explanation. This is suggested by the finding that the small tracer dye sulfonylrhodamine-B readily enters granules of B-cells, but influx of larger dextran-based tracer molecules is delayed (Takahashi et al., 2002). Thus, the rate and latency of tracer influx into the exocytosing granule depends on the molecular size of the tracer, which has been interpreted as gradual expansion of the pore. Insulin is stored in the granule as a Zn_2-insulin$_6$ crystal, and the dimensions of this crystal suggest that their release would require a pore diameter of at least 5 nm. Thus, the rate fusion pore dilation may determine the onset of peptide release. Alternatively, it can be envisioned that the insulin crystal has to be dissolved prior to release. This process may take some time and its rate depends on environmental factors. For example neutralization of the luminal pH, which we found to be delayed by 0.9 seconds with respect to fusion pore formation (Fig. 4B,D,E), results in decreased stability of the insulin crystal (Hutton,

1994). Aggregation of matrix and cargo proteins could therefore prevent release of peptides until their mobilization is triggered by a change in the ionic composition of the lumen.

Is differential release mediated via transient fusion?

Traditionally, insulin granules have been thought to collapse into the plasma membrane during exocytosis (full fusion). This may have been the case for some of the granules we studied; most notably those where the VAMP-pHluorin signal had a rapid decay phase (Figs 4, 5). However, we often observed a plateau phase in the VAMP-pHluorin signal, which indicates that the granules did not collapse immediately. Indeed, there is now good evidence that a significant fraction of granules remains structurally intact after exocytosis (Barg et al., 2002; Perrais et al., 2004; Taraska and Almers, 2004; Taraska et al., 2003; Tsuboi et al., 2004; Tsuboi et al., 2000; Vo et al., 2004). Confirming these studies, we report here that in up to two-thirds of the exocytotic events the labeled IAPP remained at the site of the granule. Furthermore, the extracellular tracer dye Alexa568 was trapped in a stimulus-dependent manner in granules that still contained the release marker IAPP-EGFP (Fig. 7). Since the molecular weight of Alexa568 (M_r 0.7) is comparable with that of ATP (M_r 0.5), it seems probable that ATP exited the granules that were filled with the dye. Together with the fact that dye accumulation was insensitive to extensive washing, this indicates that the granules had undergone exocytosis, released small compounds like nucleotides and then closed their pores to pinch off of the plasma membrane.

How is the mode of exocytosis (full fusion vs transient exocytosis) related to the mode of release from a granule (partial or complete)? It is tempting to equate transient exocytosis with partial cargo release because the duration of the transient fusion pore openings is long in relation to the time it takes for nucleotide release (Fig. 3C and Fig. 4E). In addition, we observed nucleotide release from granules engaged in transient exocytosis (Fig. 6F). This finding is in line with previous reports that chromaffin granules completely release their acetylcholine content during transient fusion (Albillos et al., 1997). By contrast, peptide release was restricted in the majority of exocytosis events (Figs 5, 6). This finding agrees with data from PC12 and Min6 cells, where exocytosis did not necessarily lead to release (Holroyd et al., 2002; Tsuboi and Rutter, 2003). Assuming that the duration of the plateau phase in VAMP-pHluorin experiments (1 second) reports the time during which the pore remains open, premature closure of the pore is a likely mechanism by which release of peptides (delay of 2.2 seconds after exocytosis) is prevented (Fig. 4). There is evidence that granules that are retrieved intact in this manner remain fusion competent and are able to bypass the endosomal recycling pathway (Vo et al., 2004). The presence of nucleotide transporters in insulin granules supports the idea that such recaptured granules can be recycled by simple refilling with the nucleotide (Bankston and Guidotti, 1996). A similar mechanism has been postulated for chromaffin granules (Tabares et al., 2001). Granule recycling by transient exocytosis and refilling with transmitter provides the cell with a secretory pathway that avoids sorting, concentration and internalization of the granular components.

While it seems plausible that such rapid endocytic retrieval of granules is achieved simply by reversal of fusion pore opening, such a mechanism is not compatible with the experimental evidence. To accommodate the large and bulky peptide hormones, the fusion pore must expand to diameters >5-10 nm, while capacitance measurements indicate that formation of the fusion pore is reversible only as long as the diameter remains below 2-3 nm (Albillos et al., 1997; Breckenridge and Almers, 1987). Thus, whenever peptide release occurs during transient exocytosis, the pore is unlikely to close by reversal of the fusion reaction. A recent study provided evidence that in Min6 cells the GTPase dynamin, but not other endocytosis-related proteins, is required for stabilization of the granule and pore closure (Tsuboi et al., 2004). It is likely that other proteins will be implicated in this process in the future. Finally, it seems plausible that B-cells would control the differential release of nucleotides and peptides depending on the metabolic state of the body. Future work should therefore address whether a defect in this regulation could underlie certain aspects of human diabetes.

We thank W. Almers (Portland, OR; supported by NIH MH-60600) for the use of equipment, B. Khakh (Cambridge, UK), J. Rothman (Sloan Kettering, USA) and R. Tsien (San Diego, USA) for supplying plasmids, D. Machado (La Laguna, Tenerife, Spain) for helpful discussion and K. Borglid for technical assistance. Supported by the Swedish Research Council (Vetenskapsrådet) Swedish Strategic Research Foundation, the Göran Gustafssons Stiftelse for Research in the Natural Sciences and Medicine, the European Foundation for the Study of Diabetes (Albert Renold Award), the Juvenile Diabetes Research Foundation, the Swedish Diabetes Association, the Crafoord Foundation, the Novo Nordisk Foundation, the Royal Physiographic Society, and Thurings Stiftelse and the Wellcome Trust. P.R. is a Royal Society Wolfson research fellow. S.B. was a recipient of an EMBO long-term fellowship during part of this study.

References

Albillos, A., Dernick, G., Horstmann, H., Almers, W., Alvarez de Toledo, G. and Lindau, M. (1997). The exocytotic event in chromaffin cells revealed by patch amperometry. *Nature* **389**, 509-512.

Ales, E., Tabares, L., Poyato, J. M., Valero, V., Lindau, M. and Alvarez de Toledo, G. (1999). High calcium concentrations shift the mode of exocytosis to the kiss-and-run mechanism. *Nat. Cell. Biol.* **1**, 40-44.

Alvarez de Toledo, G., Fernandez-Chacon, R. and Fernandez, J. M. (1993). Release of secretory products during transient vesicle fusion. *Nature* **363**, 554-558.

Angleson, J. K., Cochilla, A. J., Kilic, G., Nussinovitch, I. and Betz, W. J. (1999). Regulation of dense core release from neuroendocrine cells revealed by imaging single exocytic events. *Nat. Neurosci.* **2**, 440-446.

Aravanis, A. M., Pyle, J. L. and Tsien, R. W. (2003). Single synaptic vesicles fusing transiently and successively without loss of identity. *Nature* **423**, 643-647.

Archer, D. A., Graham, M. E. and Burgoyne, R. D. (2002). Complexin regulates the closure of the fusion pore during regulated vesicle exocytosis. *J. Biol. Chem.* **277**, 18249-18252.

Asfari, M., Janjic, D., Meda, P., Li, G., Halban, P. A. and Wollheim, C. B. (1992). Establishment of 2-mercaptoethanol-dependent differentiated insulin-secreting cell lines. *Endocrinology* **130**, 167-178.

Bankston, L. A. and Guidotti, G. (1996). Characterization of ATP transport into chromaffin granule ghosts. Synergy of ATP and serotonin accumulation in chromaffin granule ghosts. *J. Biol. Chem.* **271**, 17132-17138.

Barg, S., Ma, X., Eliasson, L., Galvanovskis, J., Göpel, S. O., Obermüller, S., Platzer, J., Renström, E., Trus, M., Atlas, D. et al. (2001). Fast exocytosis with few Ca^{2+} channels in insulin-secreting mouse pancreatic B cells. *Biophys. J.* **81**, 3308-3323.

Barg, S., Olofsson, C. S., Schriever-Abeln, J., Wendt, A., Gebre-Medhin, S., Renström, E. and Rorsman, P. (2002). Delay between fusion pore opening and peptide release from large dense-core vesicles in neuroendocrine cells. *Neuron* **33**, 287-299.

Breckenridge, L. J. and Almers, W. (1987). Currents through the fusion pore that forms during exocytosis of a secretory vesicle. *Nature* **328**, 814-817.
Ceccarelli, B., Hurlbut, W. P. and Mauro, A. (1973). Turnover of transmitter and synaptic vesicles at the frog neuromuscular junction. *J. Cell Biol.* **57**, 499-524.
Chow, R. H., von Rüden, L. and Neher, E. (1992). Delay in vesicle fusion revealed by electrochemical monitoring of single secretory events in adrenal chromaffin cells. *Nature* **356**, 60-63.
Detimary, P., Jonas, J. C. and Henquin, J. C. (1995). Possible links between glucose-induced changes in the energy state of pancreatic B cells and insulin release. Unmasking by decreasing a stable pool of adenine nucleotides in mouse islets. *J. Clin. Invest.* **96**, 1738-1745.
Han, X., Wang, C. T., Bai, J., Chapman, E. R. and Jackson, M. B. (2004). Transmembrane segments of syntaxin line the fusion pore of Ca^{2+}-triggered exocytosis. *Science* **304**, 289-292.
Hartmann, J. and Lindau, M. (1995). A novel Ca^{2+}-dependent step in exocytosis subsequent to vesicle fusion. *FEBS Lett.* **363**, 217-220.
Heuser, J. E. and Reese, T. S. (1973). Evidence for recycling of synaptic vesicle membrane during transmitter release at the frog neuromuscular junction. *J. Cell Biol.* **57**, 315-344.
Holroyd, P., Lang, T., Wenzel, D., De Camilli, P. and Jahn, R. (2002). Imaging direct, dynamin-dependent recapture of fusing secretory granules on plasma membrane lawns from PC12 cells. *Proc. Natl. Acad. Sci. USA* **99**, 16806-16811.
Hutton, J. C. (1994). Insulin secretory granule biogenesis and the proinsulin-processing endopeptidases. *Diabetologia* **37 Suppl. 2**, S48-S56.
Ivarsson, R., Obermüller, S., Rutter, G. A., Galvanovskis, J. and Renström, E. (2004). Temperature-sensitive random insulin granule diffusion is a prerequisite for recruiting granules for release. *Traffic* **5**, 750-762.
Khakh, B. S., Smith, W. B., Chiu, C. S., Ju, D., Davidson, N. and Lester, H. A. (2001). Activation-dependent changes in receptor distribution and dendritic morphology in hippocampal neurons expressing $P2X_2$-green fluorescent protein receptors. *Proc. Natl. Acad. Sci. USA* **98**, 5288-5293.
Kiang, W. L., Krusius, T., Finne, J., Margolis, R. U. and Margolis, R. K. (1982). Glycoproteins and proteoglycans of the chromaffin granule matrix. *J. Biol. Chem.* **257**, 1651-1659.
Kirshner, N., Sage, H. J., Smith, W. J. and Kirshner, A. G. (1966). Release of catecholamines and specific protein from adrenal glands. *Science* **154**, 529-531.
Lindau, M. and Almers, W. (1995). Structure and function of fusion pores in exocytosis and ectoplasmic membrane fusion. *Curr. Opin. Cell Biol.* **7**, 509-517.
Lollike, K., Borregaard, N. and Lindau, M. (1998). Capacitance flickers and pseudoflickers of small granules, measured in the cell-attached configuration. *Biophys. J.* **75**, 53-59.
MacDonald, P. E., Obermüller, S., Vikman, J., Galvanovskis, J., Rorsman, P. and Eliasson, L. (2005). Regulated exocytosis and kiss-and-run of synaptic-like microvesicles in INS-1 and primary rat β-cells. *Diabetes* **54**, 736-743.
Marszalek, P. E., Farrell, B., Verdugo, P. and Fernandez, J. M. (1997). Kinetics of release of serotonin from isolated secretory granules. II. Ion exchange determines the diffusivity of serotonin. *Biophys. J.* **73**, 1169-1183.
Michael, D. J., Geng, X., Cawley, N. X., Loh, Y. P., Rhodes, C. J., Drain, P. and Chow, R. H. (2004). Fluorescent cargo proteins in pancreatic β-cells: design determines secretion kinetics at exocytosis. *Biophys. J.* **87**, L03-L05.
Miesenbock, G., De Angelis, D. A. and Rothman, J. E. (1998). Visualizing secretion and synaptic transmission with pH-sensitive green fluorescent proteins. *Nature* **394**, 192-195.
Nanavati, C. and Fernandez, J. M. (1993). The secretory granule matrix: a fast-acting smart polymer. *Science* **259**, 963-965.
Perrais, D., Kleppe, I. C., Taraska, J. W. and Almers, W. (2004). Recapture after exocytosis causes differential retention of protein in granules of bovine chromaffin cells. *J. Physiol.* **560**, 413-428.
Regazzi, R., Wollheim, C. B., Lang, J., Theler, J. M., Rossetto, O., Montecucco, C., Sadoul, K., Weller, U., Palmer, M. and Thorens, B. (1995). VAMP-2 and cellubrevin are expressed in pancreatic β-cells and are essential for Ca^{2+}-but not for GTPγS-induced insulin secretion. *EMBO J.* **14**, 2723-2730.
Reigada, D., Diez-Perez, I., Gorostiza, P., Verdaguer, A., Gomez de Aranda, I., Pineda, O., Vilarrasa, J., Marsal, J., Blasi, J., Aleu, J. et al. (2003). Control of neurotransmitter release by an internal gel matrix in synaptic vesicles. *Proc. Natl. Acad. Sci. USA* **100**, 3485-3490.
Scepek, S., Coorssen, J. R. and Lindau, M. (1998). Fusion pore expansion in horse eosinophils is modulated by Ca^{2+} and protein kinase C via distinct mechanisms. *EMBO J.* **17**, 4340-4345.
Smith, P. A., Proks, P. and Ashcroft, F. M. (1999). Quantal analysis of 5-hydroxytryptamine release from mouse pancreatic beta-cells. *J. Physiol.* **521**, 651-664.
Spruce, A. E., Breckenridge, L. J., Lee, A. K. and Almers, W. (1990). Properties of the fusion pore that forms during exocytosis of a mast cell secretory vesicle. *Neuron* **4**, 643-654.
Tabares, L., Ales, E., Lindau, M. and Alvarez de Toledo, G. (2001). Exocytosis of catecholamine (CA)-containing and CA-free granules in chromaffin cells. *J. Biol. Chem.* **276**, 39974-39979.
Takahashi, N., Kishimoto, T., Nemoto, T., Kadowaki, T. and Kasai, H. (2002). Fusion pore dynamics and insulin granule exocytosis in the pancreatic islet. *Science* **297**, 1349-1352.
Taraska, J. W. and Almers, W. (2004). Bilayers merge even when exocytosis is transient. *Proc. Natl. Acad. Sci. USA* **101**, 8780-8785.
Taraska, J. W., Perrais, D., Ohara-Imaizumi, M., Nagamatsu, S. and Almers, W. (2003). Secretory granules are recaptured largely intact after stimulated exocytosis in cultured endocrine cells. *Proc. Natl. Acad. Sci. USA* **100**, 2070-2075.
Tsien, R. Y. (1998). The green fluorescent protein. *Annu. Rev. Biochem.* **67**, 509-544.
Tsuboi, T. and Rutter, G. A. (2003). Multiple forms of 'Kiss-and-Run' exocytosis revealed by evanescent wave microscopy. *Curr. Biol.* **13**, 563-567.
Tsuboi, T., Zhao, C., Terakawa, S. and Rutter, G. A. (2000). Simultaneous evanescent wave imaging of insulin vesicle membrane and cargo during a single exocytotic event. *Curr. Biol.* **10**, 1307-1310.
Tsuboi, T., McMahon, H. T. and Rutter, G. A. (2004). Mechanisms of dense core vesicle recapture following 'kiss and run' ('cavicapture') exocytosis in insulin-secreting cells. *J. Biol. Chem.* **279**, 47115-47524.
Uvnäs, B. and Åborg, C. H. (1988). Catecholamines (CA) and adenosine triphosphate (ATP) are separately stored in bovine adrenal medulla, both in ionic linkage to granule sites, and not as a non-diffusible CA-ATP-protein complex. *Acta Physiol. Scand.* **132**, 297-311.
Verdugo, P. (1991). Mucin exocytosis. *Am. Rev. Respir. Dis.* **144**, S33-S37.
Viveros, O. H., Arqueros, L. and Kirshner, N. (1969). Quantal secretion from adrenal medulla: all-or-none release of storage vesicle content. *Science* **165**, 911-913.
Vo, Y. P., Hutton, J. C. and Angleson, J. K. (2004). Recycling of the dense-core vesicle membrane protein phogrin in Min6 beta-cells. *Biochem. Biophys. Res. Commun.* **324**, 1004-1010.
Wang, C. T., Grishanin, R., Earles, C. A., Chang, P. Y., Martin, T. F., Chapman, E. R. and Jackson, M. B. (2001). Synaptotagmin modulation of fusion pore kinetics in regulated exocytosis of dense-core vesicles. *Science* **294**, 1111-1115.
Yang, Y., Udayasankar, S., Dunning, J., Chen, P. and Gillis, K. D. (2002). A highly Ca^{2+}-sensitive pool of vesicles is regulated by protein kinase C in adrenal chromaffin cells. *Proc. Natl. Acad. Sci. USA* **99**, 17060-17065.
Zenisek, D., Davila, V., Wan, L. and Almers, W. (2003). Imaging calcium entry sites and ribbon structures in two presynaptic cells. *J. Neurosci.* **23**, 2538-2548.
Zimmerberg, J., Curran, M., Cohen, F. S. and Brodwick, M. (1987). Simultaneous electrical and optical measurements show that membrane fusion precedes secretory granule swelling during exocytosis of beige mouse mast cells. *Proc. Natl. Acad. Sci. USA* **84**, 1585-1589.